Italian Journal of Food Science, 2025; 37 (2): 134–148

Biological synthesis of iron nanoparticles: characterization and therapeutic potential using *Grewia optiva* leaf extract

Khushbakht Asad[1], Muhammad Salman Khan[1]*, Sehrish Asad[2], Farhad Badshah[1,3], Eliana Ibánez-Arancibia[4,5], Muhammad Bilal[6], Mushtaq Ahmad Khan[7], Patricio R. De los Ríos-Escalante[5,8], Sohail Anjum[9], Hamza Badamasi[10], Christian Tuemmers[8]

[1]Department of Zoology, Abdul Wali Khan University Mardan, Mardan, Pakistan; [2]Department of Botany, Abdul Wali Khan University Mardan, Mardan, Pakistan; [3]State Key Laboratory Biotech Breeding, Institute of Animal Science, Chinese Academy of Sciences, Beijing, China; [4]PhD Program in Sciences Mentioning Applied Molecular and Cell Biology, La Frontera University, Temuco, Chile; [5]Department of Biological and Chemical Sciences, Faculty of Natural Resources, Catholic University of Temuco, Temuco, Chile; [6]Department of Zoology, Government College University Lahore, Pakistan; [7]Department of Agriculture, University of Swabi, Khyber Pakhtunkhwa, Pakistan; [8]Department of Veterinary Sciences and Public Health, Faculty of Natural Resources, Catholic University of Temuco, Temuco, Chile; [9]Department of Zoology, University of Malakand, Mardan, Pakistan; [10]Department of Chemistry, Federal University Dutse, Dutse, Nigeria

***Corresponding Author:** Muhammad Salman Khan, Department of Zoology, Abdul Wali Khan University Mardan, Mardan 23200, Pakistan. Email: salman.khan@awkum.edu.pk

Academic Editor: Prof. Valeria Sileoni—University of Mercatorum, Italy

Received: 7 October 2024; Accepted: 13 January 2025; Published: 1 April 2025

ORIGINAL ARTICLE

Abstract

Grewia optiva leaf extract was used as a reducing and stabilizing agent to create iron nanoparticles (FeNPs) in an eco-friendly manner. Before being extracted in an aqueous solution for 20 min at 100 °C using Jeldal equipment, the leaves were meticulously dried, washed, and dried again. The extract was used to dissolve iron (III) chloride ($FeCl_3$) to bio-fabricate iron nanoparticles (FeNPs). Temperature, duration, pH, and salt effect were the parameters used to optimize the bio-fabricated FeNPs. It was found that a temperature of 85°C, pH ranging from 6 to 7, and a 24-h duration were ideal for the bio-fabrication of FeNPs. The FeNPs were analyzed through various methods, i.e., Fourier-transform infrared spectroscopy (FT-IR) for the identification of chemical bonds and functional groups, X-ray diffraction (XRD) for crystalline structure, and transmission electron microscopy (TEM) for morphological analysis. Scanning electron microscopy was used to analyze the shape and size of the nanoparticles. FeNPs exhibited noteworthy biological potential through their ability to scavenge free radicals and their demonstrated phytotoxic, insecticidal, analgesic, antibacterial, and antipyretic properties. The findings showed that the aqueous extract of *Grewia optiva* contained FeNPs that could be used to create innovative pharmaceutical and agricultural medicines.

Keywords: biological activities; bio fabrication; $FeCl_3$; FeNPs; *Grewia optiva*

 ISSN 1120-1770 online, DOI 10.15586/ijfs.v37i2.2832

Introduction

Nanotechnology is a procedure to manufacture massive surface-to-volume ratios through the fabrication of particles with dimensions ranging from 1 to 100 nm. It plays a significant role in the food and pharmaceutical industries (Kalashgarani *et al.*, 2022). Nanotechnology is a rapidly growing field of study due to its multifaceted applications in biology, medicine, and engineering (Mirza *et al.*, 2018). The use of metallic nanoparticles significantly enhances the diagnosis and treatment of multiple diseases (Asad *et al.*, 2023). Among the beneficial properties of nanoparticles (NPs) are their small size, large surface area, and malleable form and morphology (Jagaran *et al.*, 2020; Sajid *et al.*, 2020). Since a wide range of promising materials have been developed by researchers worldwide, NPs can be produced with a variety of chemical compositions. Formulations based on polymeric, liposomal, inorganic, or hybrid nanomaterials have been the subject of extensive research in recent years as potential novel tools for the diagnosis and treatment of different types of illnesses (Omidian *et al.,* 2023, Păduraru *et al.,* 2022). Smaller metal-based NPs (sizes ranging from 10 to 100 nm) combine with biomolecules inside and on the upper surface of cells due to their distinctive electrical and optical properties. A variety of functional groups, such as peptides, antibodies, medications, enzymes, RNA, and DNA, can be added to the surface, in addition to polymers that might be biocompatible, to target various cells (Younis *et al.*, 2021; Chopra *et al.*, 2022). Green synthesis based on plants and materials obtained from plants is extensively available and has large-scale production potential (Iftikhar *et al.*, 2020). Iron nanoparticles, in particular, are attracting a lot of attention because of their special qualities, i.e., high surface-to-volume ratio, simple separation techniques, and super-paramagnetic behavior. Magnetic nanoparticles (NPs) with proper surface chemistry have been produced using a variety of physical, chemical, and biological methods (Prakash *et al.,* 2024). Because of their minute physical characteristics, which include superparamagnetic properties, stability in liquid solutions, low sensitivity to oxidation, and flexible surface chemistry, iron oxides are the most highly biocompatible metal oxide nanoparticles. These characteristics have a broad range of applications in environmental regulation, such as the degradation of antibiotics, dye adsorption, food-related processes, biomedical applications (drug delivery), magnetic cell sorting, magnetic resonance imaging (MRI), oncology, magnetic particle imaging (MPI), immunoassays, and tissue engineering. Antimicrobial activity against a variety of pathogens, including bacteria, fungi, and ROS, demonstrates the great potential of *Grewia optiva* (Priya *et al.*, 2021). *Grewia optiva* is an antibacterial, analgesic, antioxidant, and anticholinesterase plant belonging to the Malvaceae family. Its phytochemical profile has been studied by several authors, and they have identified several biomedically significant alkaloids, saponins, tannins, flavonoids, and terpenoids. Due to its secondary metabolites, which have promising bioactive potential, this plant is an excellent choice for the fabrication of NPs (Iftikhar *et al.,* 2020). *Grewia* species hold significant promise for treating or preventing various chronic illnesses due to their abundance of phytochemicals. There are approximately 159 species of *Grewia* found in the tropical and subtropical regions of Pakistan, India, China, Malaysia, South Africa, Australia, northern Thailand, and Nigeria (Qamar *et al.*, 2021). The present work aimed to synthesize FeNPs in a single step using *Grewia optiva* leaf extract. Multiple techniques, including TEM analysis, SEM, FTIR spectroscopy, EDX, and XRD, were used to investigate the produced FeNPs. Their scavenging, phytotoxic, antibacterial, antifungal, insecticidal, analgesic, and antipyretic properties were evaluated to further investigate the biological potential of the nanoparticles.

Methodology

Collection of plant material

Fresh *Grewia optiva* leaves were collected from Upper Dir and identified by the Department of Botany (Abdul Wali Khan University Mardan) (Figure 1). The leaves were cleaned with water and left to dry in a shaded area for 1 week. The leaves were then dried, ground into powder, and stored in a cool, dry area for experimental purposes (Asad *et al*., 2022).

Plant extraction

A total of 25 g of powdered leaves were dissolved in 100 mL of distilled water and heated to boiling for 20 min at 60°C in a Jeldal apparatus to prepare the aqueous extract. Whatman paper was used to filter the sample, and the sample was stored in a refrigerator for experimental purposes (Asad *et al*., 2022).

Figure 1. ***Grewia optiva*** **leaves.**

Synthesis of iron nanoparticles (FeNPs)

To synthesize FeNPs, 1 mM of $FeCl_3$ was added to a flask along with a biological reducing agent (leaf extract from *Grewia optiva*), and the mixture was stirred for 24 h using a magnetic stirrer. The color changed from creamy to greenish-black, indicating the reduction of iron ions and the synthesis of NPs. $FeCl_3$ levels were increased at each step in the following ratios: 1:1, 1:2, 1:3, 1:4, 1:5, and 1:6, respectively. UV spectroscopy was used to evaluate the absorbance of the synthesized sample (Xu *et al*., 2022).

Optimizations

Time duration

The time duration (synthesis time) was used to optimize the synthesized samples, such as FeNPs. Samples were optimized for 30 min, 60 min, 90 min, and 24 h. The absorbance of each sample was evaluated using UV spectroscopy after the allotted time (Asad *et al*., 2022).

Temperature effect

The absorbency of the synthesized FeNPs was determined by UV spectrometry. Each sample was exposed to one of the following temperatures: room temperature, 35 °C, 50 °C, 65 °C, 80 °C, and 95 °C for 10 min, respectively (Asad *et al.,* 2022).

Salt (NaCl) effect

Salt concentrations were used to optimize the synthesized FeNPs. A 1 mM NaCl solution was prepared in 20 mL distilled water. Various salt concentrations (i.e., 0.2, 0.4, 0.6, 0.8, and 1 mL) were added to each vial containing the FeNPs solution, respectively. The absorbance of the samples was measured using double-beam UV spectrophotometry (Asad *et al*., 2022).

pH effect

The formation of NPs is influenced by pH parameters. For this purpose, 0.1 N HCl and 0.1 N NaOH solutions were prepared. Vials were used to determine the pH of FeNPs. Three milliliters of FeNPs solutions were added to each vial. The pH was varied according to the following parameters: 1–2, 2–3, 3–4, 4–5, 7, 8, 8–9, 10, and 11–12, respectively. After the reaction was completed, UV spectrophotometry was used to measure the absorbance of all samples (Asad *et al*., 2022).

Characterization

UV spectrophotometry

Grewia optiva leaf extract was used as a reducing agent in the bio-fabrication of FeNPs, and the absorbance was measured using UV spectrophotometry. The absorbance of the derived mono- and bimetallic nanoparticles was measured with distilled water serving as a reference. Reaction mixtures containing leaf extract and salts (iron III chloride) solution in different ratios (i.e., 1:1, 1:2, 1:3, 1:4, 1:5, and 1:6) were analyzed over a wavelength range of 300–800 nm (Acay *et al*., 2021).

FT-IR spectrophotometry

Using a vacuum dryer, the FeNPs were fully dried at 37°C. The synthesized particles were mixed with KBr and compacted using a hydraulic pellet press to produce sample pellets. The "PerkinElmer Spectrometer FT-IR SPECTRUM ONE" was used to analyze the samples for FT-IR spectroscopy, with a resolution of 4 cm^{-1} and a range of 4000 cm^{-1} to 0 cm^{-1} (Acay *et al*., 2021).

X-ray diffraction assay

FeNPs were examined through an X-ray diffraction pattern using an X-ray diffractometer, JEOL JDX 3532. A nickel monochromator cleans the wave through a tube with a voltage of 40 kV and a current of 30 mA, using Cu-K radiation. The line width of the highest intensity reflection peak was used to calculate the average diameter of the NPs. Scherr's equation was utilized to compute the FeNPs' sizes, yielding the following formula: $D = K\lambda / (\beta_{1/2} \cos\theta)$ (Acay *et al*., 2021).

Scanning electron microscopy

Grewia optiva leaf extract was used to prepare the FeNPs. Following fabrication and thorough drying, a small quantity was placed on a carbon-coated SEM grid, left to dry, and then coated with metal using a Spi-module sputter coater. Scanning electron microscopy (JSM-5910-JEOL) was used to examine the morphological characteristics of the metal-coated NPs (Mofolo *et al*., 2020).

Transmission electron microscopy (TEM)

Grewia optiva leaf extract was used to prepare the FeNPs. Following fabrication and thorough drying, a small quantity was placed on a carbon-coated TEM grid, allowed to dry, and then coated with metal using a Spi-module sputter coater. Transmission electron microscopy (JSM-5910-JEOL) was then used to examine the morphological characteristics of the metal-coated NPs (Mofolo *et al.,* 2020).

Biological assays

Antifungal assay

Aspergillus Niger and *Alternaria Solana* fungal strains were obtained from the Microbiology Laboratory at Abdul Wali Khan University Mardan. All apparatuses were autoclaved and sterilized at 121°C. Twenty milliliters of autoclaved, molten, and cooled media (PDA) were taken, placed in sterile Petri plates, and allowed to

solidify at room temperature. The plates were kept for 24 h. The fungal strains were streaked onto the media, and four wells were formed in each plate using a sterilized borer. All wells were labeled with the respective samples. DMSO and clotrimazole acted as negative and positive controls, respectively. The plates were incubated at 28±1°C for a week. Growth was measured by the inhibition zone (mm) in the media (Keshari *et al*., 2020).

Phytotoxic assay

To assess the phytotoxic potential of the FeNPs isolated from the aqueous leaf extract of *Grewia optiva*, experiments were conducted in Petri plates with three different concentrations (50 µL/mL, 100 µL/mL, and 500 µL/mL). The Petri plates were autoclaved at 121°C for 24 h. *Lamina minor* was used in the experiments, with eight plants per Petri dish. One gram of FeNPs was mixed in 1 mL of distilled water to form stock solutions. Fifty µL/mL, 100 µL/mL, and 500 µL/mL of the solution were pipetted from the stock solution and added to the Petri dishes containing *L. minor* plants. Fifteen milliliters of E-medium were added to each flask. Atrazine was used as a standard drug. Plants were checked daily during the incubation period. The Petri dishes were placed in a growth cabinet for one week. The number of fronds per Petri dish was measured and recorded on the seventh and tenth days. The results were analyzed as growth regulation in terms of percentage, as presented by (Dastagir *et al*., 2013).

$$\%\text{inhibition} = \frac{\text{control} - \text{sample}}{\text{control}} \times 100$$

Insecticidal activity

FeNPs were assessed for insecticidal potential using *Tribolium castaneum* as test insects. Under sterilized conditions, three replications of FeNPs were taken in Petri dishes. The filter sheets were cut and fitted into Petri plates, each with a size of 9 cm (90 mm). One milligram of extract was dissolved in 1 mL of distilled water, acting as a stock solution (1000 ppm). Three concentrations (100 µL/mL, 500 µL/mL, and 1000 µL/mL) of each sample were prepared. The plates were left for 24 h at room temperature, allowing the samples to evaporate completely. Once the samples had fully evaporated, 30 healthy insects, supplied by the pharmacognosy lab, were transferred to each plate using a clean brush. All plates were examined daily during the incubation period. The number of insects per Petri dish was measured and recorded on the 3rd and 7th days. The percentage was calculated using the following formula (Alisha and Thangapandiyan 2019).

$$\text{Mortality } (\%) = \frac{100 - \text{Number of insects alive in a test}}{\text{Total number of insects (control)}} \times 100$$

Bacterial assay

The Kirby-Bauer method was used to study the antibacterial potential of *Grewia optiva* and FeNPs. Test samples (*Grewia optiva* leaf extract and FeNPs) were prepared in various concentrations (50 µL/mL, 100 µL/mL, and 500 µL/mL). All equipment, as well as the nutrient agar, were sterilized in an autoclave for approximately 90 min at 121°C and 17 lb Pascal. Using a micropipette, 10 microliters of bacterial suspension were applied to the solid media and spread with a glass spreader. Four wells were created in the medium, each containing a distinct concentration of extract and FeNPs. The positive and negative controls were streptomycin and distilled water, respectively. The plates were incubated for 24 h. Inhibition zones were measured using a standard scale (Keshari *et al*., 2020).

Antioxidant assay

The antioxidant potency of the extract and FeNPs was analyzed using 1,1-diphenyl-2-picrylhydrazyl (DPPH). A DPPH solution (0.004% w/v) was prepared in methanol. In test tubes, 50 µL/mL, 100 µL/mL, and 500 µL/mL concentrations of the samples (*Grewia optiva* leaf extract and FeNPs) were mixed with 2 mL of the DPPH solution (0.004% w/v) to make a total volume of 3 mL. The mixture was incubated for 1 h at room temperature in complete darkness. The absorbance of the samples was measured using a UV spectrophotometer at 517 nm against a blank methanolic solution (Khan *et al*., 2018).

Antioxidant potential % was found out by using this formula:

$$\text{Antioxidant potential } (\%) = \frac{\text{Absorbance of control (nm)} - \text{Absorbance of test (nm)}}{\text{Absorbance of control}} \times 100$$

Analgesic assay

An acetic acid-induced writhing test was used to assess the potential of *Grewia optiva* leaf extract and FeNPs in alleviating pain. The experimental study was approved by the Ethical Committee of Abdul Wali Khan University Mardan, KPK (Pakistan). Six groups of Swiss albino mice were equally distributed. The first group of experimental animals was injected with 1 mL of normal saline (1% v/v) as a control group. The second group received only acetic acid injections and was treated as the disease group. In the following groups (3rd, 4th, 5th, and 6th), all mice received 1 mL of acetic acid injection. Writhing was counted for 5 min following a 10-min injection. Mice in the third group were given a 1 mL injection of paracetamol solution. FeNPs at 50 µL/mL, 100 µL/mL, and 500 µL/mL doses were administered to the mice in the fourth, fifth, and sixth groups, respectively, along with a 1 mL leaf aqueous extract solution. The percentage

inhibition rate of the tested samples was measured using the following formula (Shah *et al.,* 2021).

$$\text{Inhibition (\%)} = \frac{\text{Number of writhing in test group}}{\text{Number of writhing in the control group}} \times 100$$

Anti-pyretic assay

The anti-pyretic efficacy was assessed using albino mice with pyrexia induced by Brewer's yeast. Mice were given a subcutaneous injection of a 10% aqueous Brewer's yeast solution at a dose of 10 mL/kg to induce pyrexia. Before the application of the yeast solution, the body temperature of each mouse was measured using a lubricated rectal thermometer. The mice's body temperature was taken again after 18 h. Each mouse was treated intraperitoneally with the medication, and the body temperatures were measured every hour for 4 h (Sulaiman *et al*., 2022).

Result and Discussion

Iron nanoparticles synthesis

The aqueous extract was mixed with a 1 mM $FeCl_3$ solution, and the synthesis of FeNPs occurred when the color of the solution changed from creamy to greenish-black (Figure 2). The greenish-black color formation was due to the conversion of Fe^+ ions into elemental iron with size ranges in the nanometer scale. In FeNPs, the reduction of Fe^+ to nanoparticles is facilitated by metabolites such as flavonoids, proteins, carbohydrates, enzymes, phenols, and others present in plants. The greenish-black coloration is attributed to the excitation of surface plasmon resonance, indicating the fabrication of iron nanoparticles.

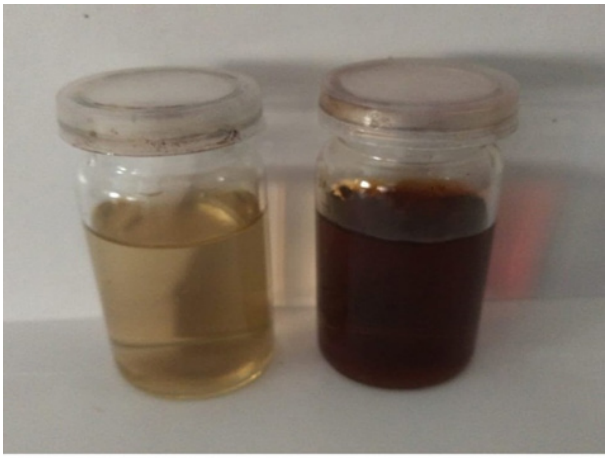

Figure 2. The dark brownish color indicates the synthesis of FeNPs.

Optimization

Optimization is crucial for controlling the size of metallic nanoparticles. Parameters such as pH, temperature, and salt concentration play an effective role in the synthesis process. These parameters were examined for their impact on controlling the size of the nanoparticles. In the optimization of the pH parameter, the experiment was conducted in two phases (acidic and basic). pH values were set at 1-2, 2-3, 3-4, 4-5, 5-6, 7, 7-8, 8-9, 9-10, 10-11, and 11-12. All samples were stirred for 3 h on a magnetic stirrer, and absorbance was measured using UV spectrophotometry. (Figure 3A). The effect of temperature on the synthesis of FeNPs was also assessed, and the results indicated that temperature significantly influences the fabrication of FeNPs. UV absorbance data showed that the absorbance peak of FeNPs increased with a rise in temperature. The lowest peak was observed at room temperature, while the highest peak was seen at 95°C. The results concluded that 95°C was the most favorable temperature for FeNPs synthesis because the highest peak was observed at this temperature (Figure 3B). From the absorbance results, it was observed that acidic pH showed good peaks, with the highest peaks observed at neutral pH and pH 6. As the pH became more acidic, the peaks also increased. The highest peak for FeNPs was observed at pH 6-7, indicating that acidic to neutral pH is favorable for FeNPs synthesis. Basic pH reduced the peak, disrupting the synthesis of FeNPs (Figure 3C). When optimizing salt concentration in FeNPs synthesis, different concentrations of salt solutions were added to the FeNPs solutions, and their absorbance was measured using UV spectroscopy. The results showed that salt concentration significantly affects the synthesis of FeNPs. As the salt concentration increased, a reduction in peak absorbance was observed. The highest peak was recorded at a 0.2 mL salt concentration, while the minimum absorbance was observed at a 1 mL salt concentration. This result indicates that lower salt concentrations are favorable for FeNPs synthesis, whereas higher salt concentrations reduce the synthesis rate of FeNPs (Figure 3D). The time period also contributed to the increase in nanoparticle synthesis, as shown in (Figure 3E).

Hammad *et al*. (2022) suggested that FeNPs were detected through UV-vis analysis. A change in color was observed due to the reduction of Fe^+ ions from ferrous sulfate. The FeNPs absorption peak occurred around 240 nm, with absorbance peaks in the region of 210-260 nm.

Ebrahiminezhad *et al*. (2017) reported that UV-vis spectroscopy for biosynthesized FeNPs using *Urtica dioica* extract showed absorption in the range of 216-265 nm. Akhbari *et al*. (2018) studied FeNPs and observed two absorption peaks at wavelengths around 216 and 284 nm.

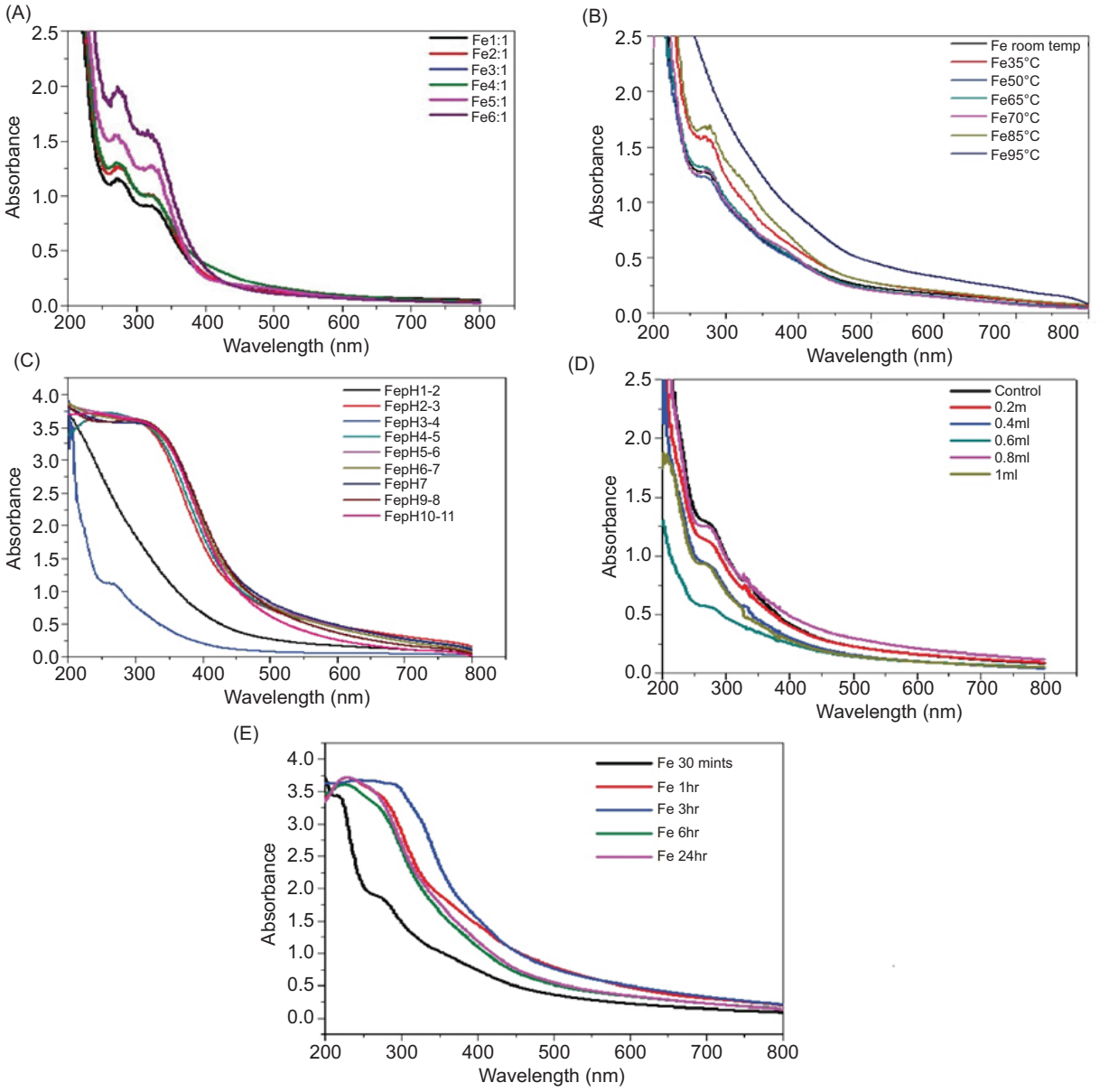

Figure 3. (A) UV-visible spectroscopy (B) pH, and (C) temperature effects on FeNPs synthesized from *Grewia optiva* leaves.

Characterization

FTIR

FeNPs prepared using *Grewia optiva* were evaluated through FT-IR analysis to identify the biomolecules of reducing agents involved in the reduction and capping of $FeCl_3$. As the iron nanoparticles are reduced and capped by the leaf extract of *Grewia optiva*, FT-IR spectroscopy of the leaf extract was also performed. FT-IR spectroscopy of the leaf extract showed peaks at 3284.2 cm^{-1}, 1969 cm^{-1}, 3070.12 cm^{-1}, 1492 cm^{-1}, 1184 cm^{-1}, and 1036 cm^{-1}. The shifted bands observed in the leaf extract indicated that the peak at 3284.2 cm^{-1} corresponds to the N-H group of primary amines, 3070.39 cm^{-1} for the C-H bond, 1969.9 cm^{-1} for the C-H bond, and 1184.94 cm^{-1} for the C=C bond. FT-IR spectroscopy of FeNPs reduced and capped by the leaf extract showed bands at 3276 cm^{-1}, 2922.1 cm^{-1}, 2850.8 cm^{-1}, 1636.9 cm^{-1}, and 1535.9 cm^{-1}. These shifts were attributed to the N-H group, C-H bond, O-H group of alcohol, C=C bond, and alkanes, respectively (Figure 4A). The identification of carbonyl groups suggests the presence of flavonoids, which bind to the metal nanoparticle surface via bonding with the alpha electrons of the carbonyl group. This bonding occurs in the absence of chelating agents. It is also observed that carbonyl groups derived from proteins and amino acids have a strong affinity for metal nanoparticles, either attaching to them or acting as stabilizers and caps (Asad *et al*., 2022).

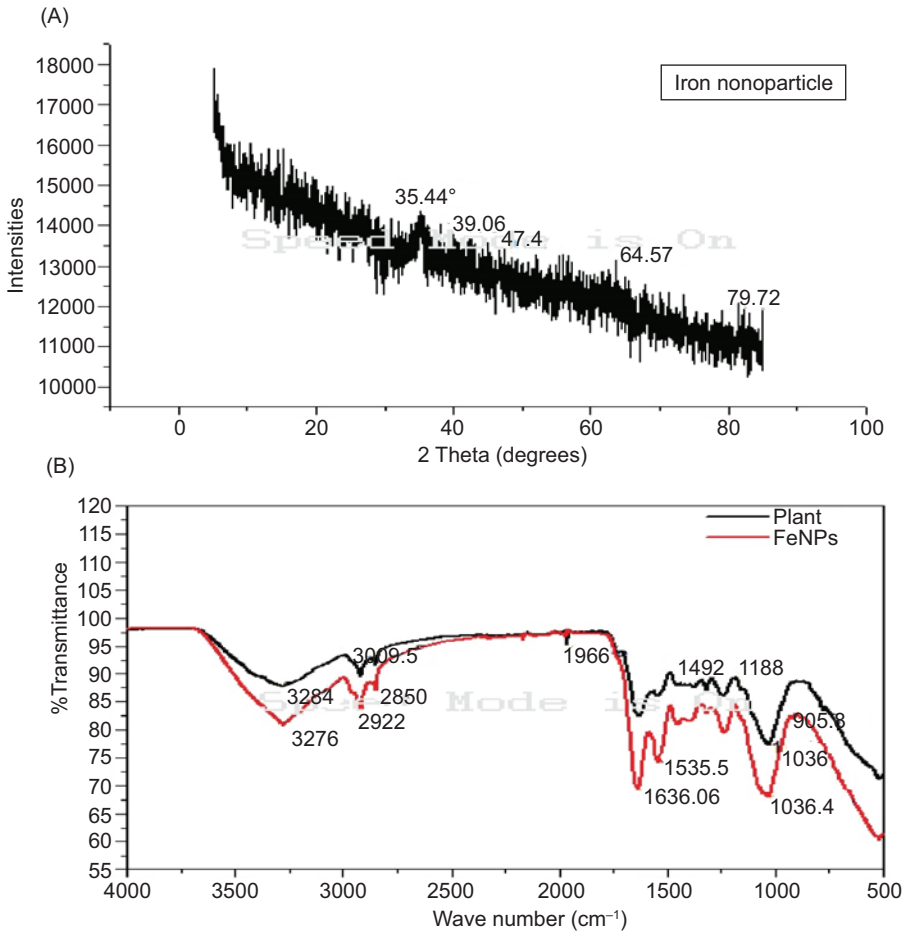

Figure 4. (A) FTIR and (B) XRD analysis of FeNPs synthesized using *Grewia optiva* leaves.

Wei *et al.*, (2016) demonstrated that the peel of *Citrus maxima* contains various peaks at 3292.84, 2927.78, 1638.55, 1350.99, and 1026.60 cm^{-1} in FeNPs.

Akhbari *et al.,* (2018) identified the presence of stabilizing and reducing agents during the synthesis of FeNPs, showing functional groups such as aliphatic amines, phenols, and organic acids.

Karpagavinayagam and Vedhi (2019) reported the presence of peaks at 3422, 2923, 2853, 1630, 618, and 467 cm^{-1} when using the flower extract of *Avicennia marina* in iron nanoparticle synthesis.

Dash *et al.,* (2019) observed the presence of peaks at 3700, 3400, 2918, 2360, 1000, 800, 717, 623, 557, and 443 cm^{-1} in iron nanoparticles synthesized using *Peltophorum pterocarpum* extract.

Sandhya *et al.,* (2021) reported that in the IR spectrum of iron oxide nanoparticles, the band at 3271 cm^{-1} is attributed to hydroxyl groups, while the band at 2962 cm^{-1} is considered indicative of carboxylic acid. The carbonyl band is located at 1605 cm^{-1}, and the band at 1065 cm^{-1} is associated with C=C bonds.

Demirezen *et al.,* (2019) found that the infrared spectra of iron oxide nanoparticles indicate that magnetite is identified by bands between 400 and 570 cm^{-1}, while haematite is identified by bands between 470 and 540 cm^{-1}.

X-ray diffraction spectroscopy

X-ray diffraction (XRD) is a crystallographic technique used to identify the crystalline nature of atomic and molecular structures. It is particularly useful for verifying the crystallinity, internal organization, and mixing of metals and their nanoparticles. During XRD analysis, a beam of incident X-rays interacts with the crystal lattice, causing diffraction in various directions. According to Bragg's law, the XRD results confirmed that the iron nanoparticles have a face-centered cubic (FCC) structure. The crystallographic analysis showed that the FCC iron nanoparticles have diffraction peaks at 39.06°, 47.44°, 64.57°, and 79.72°. These peaks correspond to the (111),

(200), (220), and (311) planes, respectively (Figure 4B). The results also indicated lattice plane formation with no evidence of impurities, and the broadening of the peaks suggests the presence of fine nanoparticles.

Demirezen *et al.,* (2019) suggested that the XRD peaks 16° and 21° correspond to the crystal face reflection of γ-Fe2O3.

Nahari *et al*. (2022) reported that the XRD analysis revealed distinct peaks at various diffraction angles, including 21.87°, 29.85°, 30.76°, 40.40°, 43.42°, and 46.18°. These angles correspond to the crystalline structure of the material. Based on these diffraction patterns, the iron nanoparticles were confirmed to be crystalline in nature. Additionally, the average diameter of the produced nanoparticles was found to be 136.43 nm, further confirming their nanoscale size as determined by the XRD analysis.

Liu *et al*. (2014) demonstrated that the XRD peaks at 14°, 27°, and 49° corresponded to the lepidocrocite form of iron oxide. Similarly, Bhuiyan *et al*. (2020) observed peaks at 26.16°, 35.12°, 36.63°, and 40.64° for α-Fe_2O_3 nanoparticles, further confirming the crystalline structure of the material.

Scanning electron microscopy (SEM)

To assess the size, morphology, and shape of the biofabricated FeNPs at different magnifications, scanning electron microscopy (SEM) was utilized. The SEM images revealed the presence of FeNPs with various shapes, including rod-shaped, spherical, and irregularly shaped particles. Aggregation of FeNPs was also observed in certain areas of the micrograph. SEM analysis indicated that the reduction process primarily took place on the surface of the particles (Figure 5A,B).

The micrograph results showed that the aggregation of FeNPs was due to the immobilization of enzymes (Sultana *et al*., 2022). Agglomeration was also observed in certain areas of the SEM micrographs. According to Ahmed *et al*. (2020), intermolecular interactions, such as Van der Waals forces between particles, are responsible for these agglomerations. Üstün *et al*. (2022) determined the particle size to be in the range of 43–57 nm. The agglomerated nanoparticles exhibited multiple forms. The agglomeration could be attributed to hydrogen bonding in the bioactive molecules, the lower capping ability of the leaf extract, or the presence of various bioactive reducing agents.

Transmission electron microscopy (TEM)

Transmission electron microscopy (TEM) is a powerful tool used to measure and analyze nanoparticle sizes. In this study, TEM was employed to evaluate the size of the FeNPs at various magnifications. Iron nanoparticles were synthesized using an extract from the leaves of

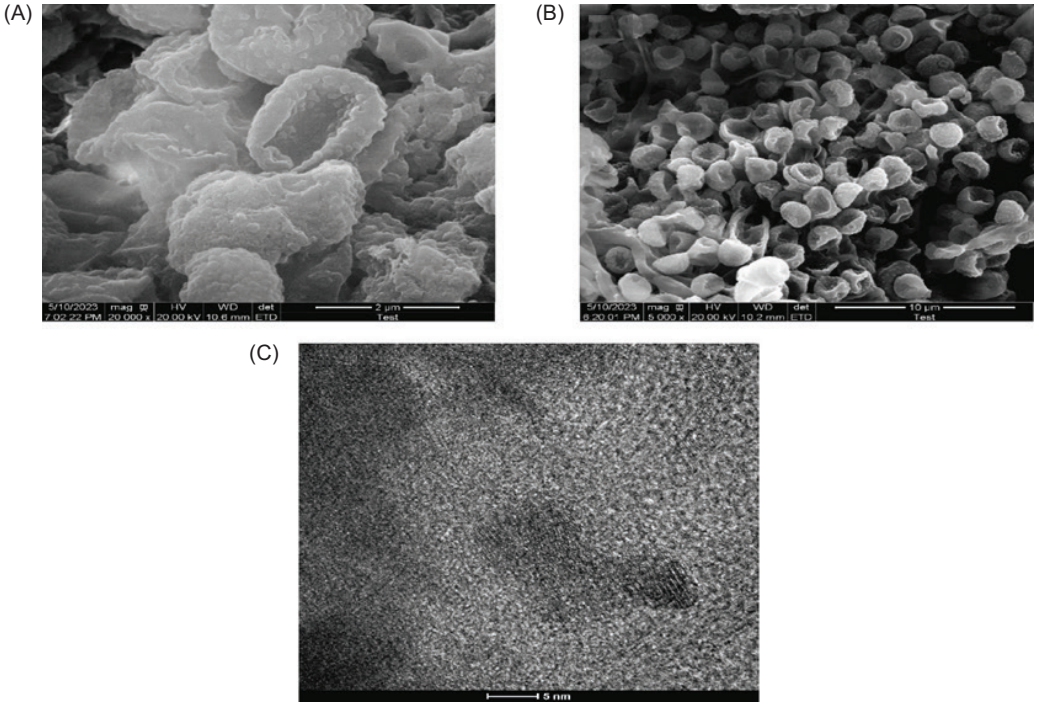

Figure 5. (A, B) SEM and (C) TEM images of FeNPs synthesized using *Grewia optiva* leaves.

Grewia optiva, and the results showed that the FeNPs had sizes ranging from 12 to 18 nm (Figure 5C).

TEM analysis of FeNPs synthesized using henna leaf extract and a $FeSO_4$ solution was performed, as reported by Naseem *et al*. (2015). The iron nanoparticles produced with henna leaf extract were found to be 21 nm in size. In contrast, when using Gardenia leaf extract, the particle size was recorded at 32 nm. Hooda *et al*. (2020) observed that green Fe_2O_3 NPs are primarily spherical, electron-dense particles with an average size of 40 nm and a size range from 15 to 80 nm, as seen in TEM images.

Biological assays

Antibacterial assays

The antibacterial activity of *Grewia optiva* leaf extract and FeNPs was assessed using the well diffusion method against *Klebsiella pneumoniae* and Escherichia coli. The results showed that the leaf extract at 500 µL/mL exhibited a significantly higher zone of inhibition (4.9 mm) against Escherichia coli ($p<0.0001$), while the lowest zone of inhibition (2 mm) was observed against *Klebsiella pneumoniae*. Similarly, FeNPs at 500 µL/mL showed a significantly larger zone of inhibition (5.7 mm) against Escherichia coli ($p<0.0001$) and the smallest zone of inhibition (4.4 mm) against *Klebsiella pneumoniae* at 100 µL/mL. Streptomycin, used as a standard antibiotic, showed a significant inhibition zone ($p<0.0001$), with the largest zone of inhibition (3.6 mm) against Escherichia coli and the smallest (3 mm) against *Klebsiella pneumoniae* (Figure 6).

Hammad *et al*. (2022) reported that Fe_2O_3-NPs exhibit a strong inhibitory effect against a variety of pathogenic bacteria. The inhibition zones caused by Fe_2O_3-NPs against *Staphylococcus aureus*, *Bacillus subtilis*, *Escherichia coli*, and *Pseudomonas aeruginosa* were found to be 26.5 mm, 24.8 mm, 19.5 mm, and 17 mm, respectively. The data indicated that gram-positive bacteria (*S. aureus* and *B. subtilis*) were more susceptible to the effects of Fe_2O_3-NPs than gram-negative bacteria (*E. coli and P. aeruginosa*).

Roy *et al*. (2022) reported that a gram-negative *Escherichia coli* bacterial culture was used to assess the antibacterial activity of FeNPs synthesized from

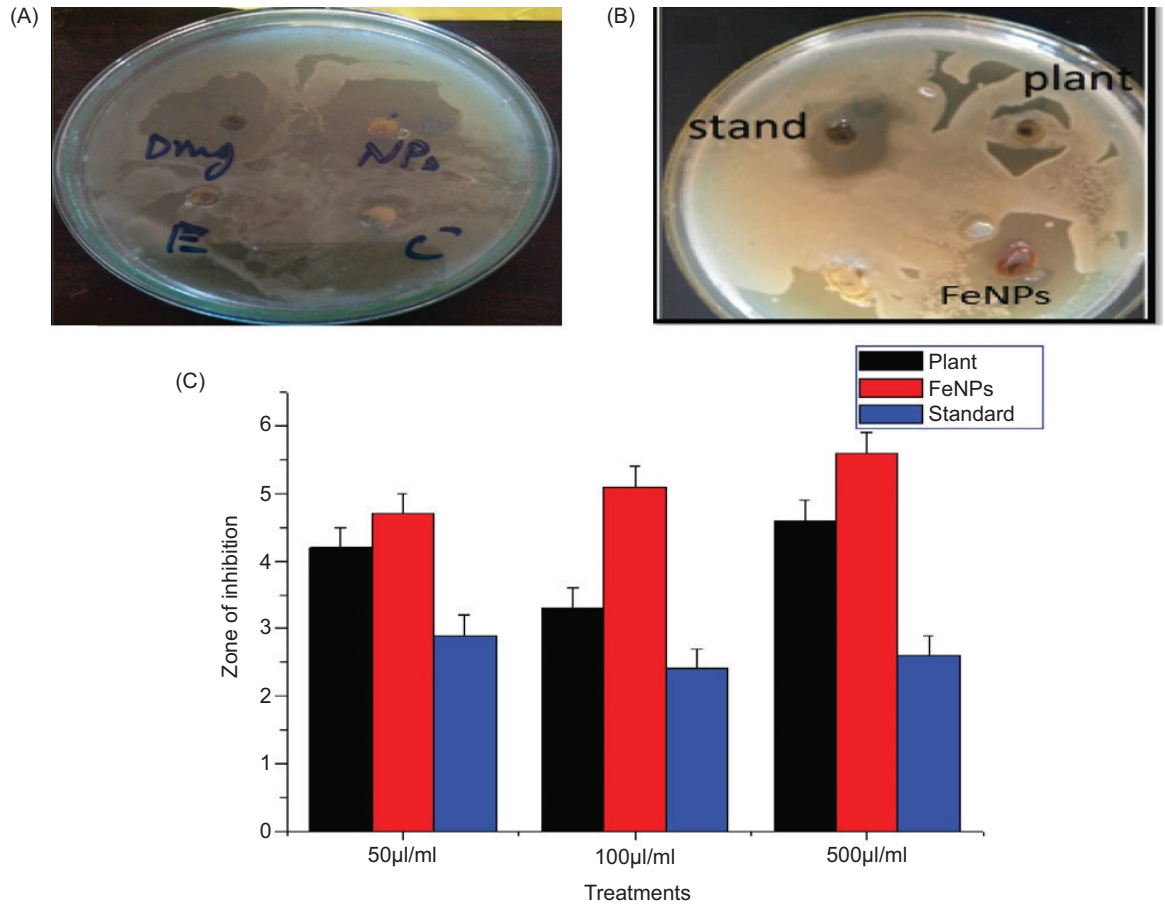

Figure 6. (A, B) Antibacterial activity and (C) Graph of FeNPs synthesized using *Grewia optiva* extract.

Catharanthus roseus. The study showed that as the concentration of FeNPs increased, the zone of inhibition also increased. The minimum zone of inhibition was observed with 10 µL of the FeNPs solution, while the maximum inhibition was observed with 30 µL. The zone containing 30 µL of FeNPs had the largest diameter at 15 mm, followed by 20 µL with a 12 mm zone, 10 µL with a 9 mm zone, and 11 mm for streptomycin.

Dash *et al*. (2019) demonstrated that the synthesis of magnetite nanoparticles using *Peltophorum pterocarpum* pod extract exhibited antibacterial activity against *Escherichia coli*. The zone of inhibition observed for *Staphylococcus epidermidis* was 16 mm, while the maximum inhibition against *E. coli* was 20 mm.

Buarki *et al.,* (2022) reported that iron oxide nanoparticles synthesized using a 1:2 volume ratio demonstrated a maximum bacterial growth inhibition of 3 mm against *Staphylococcus aureus*.

Antifungal activity

The antifungal potential of *Grewia optiva* leaf extract and FeNPs was assessed using the well diffusion method against *Aspergillus niger*. The results showed that the leaf extract exhibited the highest zone of inhibition (4.6 mm) at a concentration of 500 µl/mL, followed by clotrimazole (a standard antifungal drug), which showed the highest zone of inhibition (2.7 mm) at the same concentration. The FeNPs demonstrated a maximum zone of inhibition (5.7 mm) at 500 µl/mL, with 4.3 mm at 100 µl/mL and the least zone of inhibition (3.8 mm) at 50 µl/mL (Figure 7).

Anti-oxidant activity

The antioxidant activity of *Grewia optiva* leaf extract and FeNPs was assessed by comparing their effects to antioxidant drugs such as ascorbic acid. The percentage inhibition of DPPH radicals was calculated using the following formula:

$$\text{Percent Inhibition \%} = \frac{\text{Absorbance of Control} - \text{Absorbance of test}}{\text{Absorbance of Control}} \times 100$$

The maximum DPPH inhibition potential was significantly ($p<0.0001$) observed in FeNPs, with the highest inhibition (76.82%) at 500 µl/mL and the least inhibition (65.7%) at 50 µl/mL. *Grewia optiva* leaf extract showed a percent inhibition of 72% at 500 µl/mL, with the least inhibition (69%) at 50 µl/mL. Ascorbic acid exhibited the highest significant ($p<0.0001$) inhibition at 77.4% (Figure 8A).

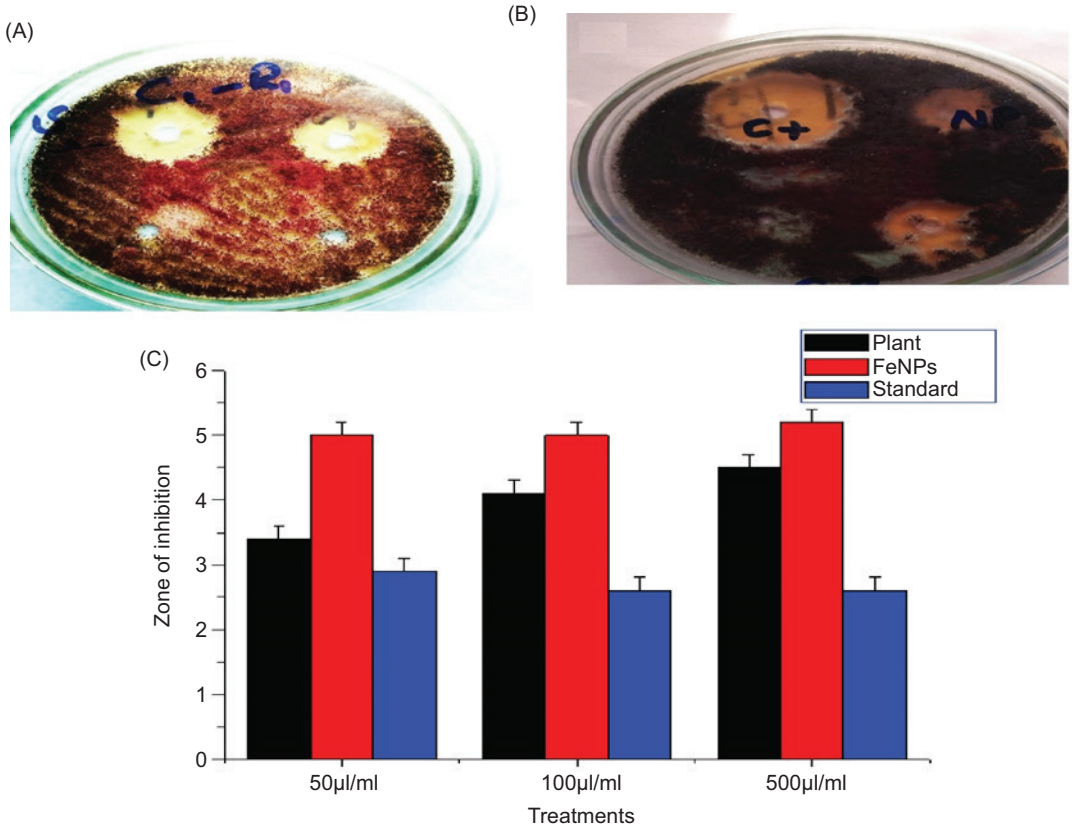

Figure 7. (A, B) Anti-fungal activity and (C) graph of FeNPs synthesized using *Grewia optiva* leaves.

Üstün et al. (2022) determined that the synthesized nanoparticles possessed impressive antioxidant activity. To assess the product's capacity to capture free radicals, the DPPH test was used. The results showed that one gram of nanoparticles exhibited antioxidant activity equivalent to 5.14 mg of ascorbic acid.

Nahari *et al.,* (2022) reported that the FRAP assay was used to evaluate the antioxidant potential of leaf extracts of *V. leucoxylon* and its FeNPs, with ascorbic acid serving as the standard. The results showed that higher concentrations of both the standard and FeNPs led to increased levels of antioxidant absorption. This trend was observed with the aqueous leaf extracts of *V. leucoxylon* as well.

Analgesic activity

To evaluate the pain-relieving capabilities of the samples, an acetic acid-induced writhing test was performed. Four replicates of the samples at different concentrations (50µl/mL, 100µl/mL, and 500µl/mL) were prepared. The leaf extract of *Grewia optiva* showed the highest significant ($p<0.0001$) percent inhibition at 500µl/mL, with a percent inhibition of 62.5%. The inhibition was slightly lower at 100µl/mL, with a percent inhibition of 60%. FeNPs at 500µl/mL demonstrated the highest percent inhibition, which was 63%, followed by 62% inhibition at 50µl/mL. The standard drug paracetamol also showed a significant ($p<0.0001$) percent inhibition of 51.5% (Figure 8B).

Tan *et al.* (2023) observed distinct writhing series over a 30-min period. Mice treated with Fe_3O_4-GA/Ag NP nanocomposite had their response times measured in the hot plate test. The objective of this test was to evaluate the typical animal response to a pinprick by intradermally injecting 0.3 mL of Fe_3O_4-GA/Ag NP nanocomposite and normal saline (0.9%) on the left and right sides of the mice's bodies, respectively.

Insecticidal assay

The insecticidal potential of FeNPs and leaf extract (Grewia optiva) was assessed against *Tribolium castaneum* at various concentrations (50 µl/mL, 100 µl/mL, and 500 µl/mL). The FeNPs demonstrated greater efficacy against *Tribolium castaneum* compared to the plant extract. The results showed that the highest mortality

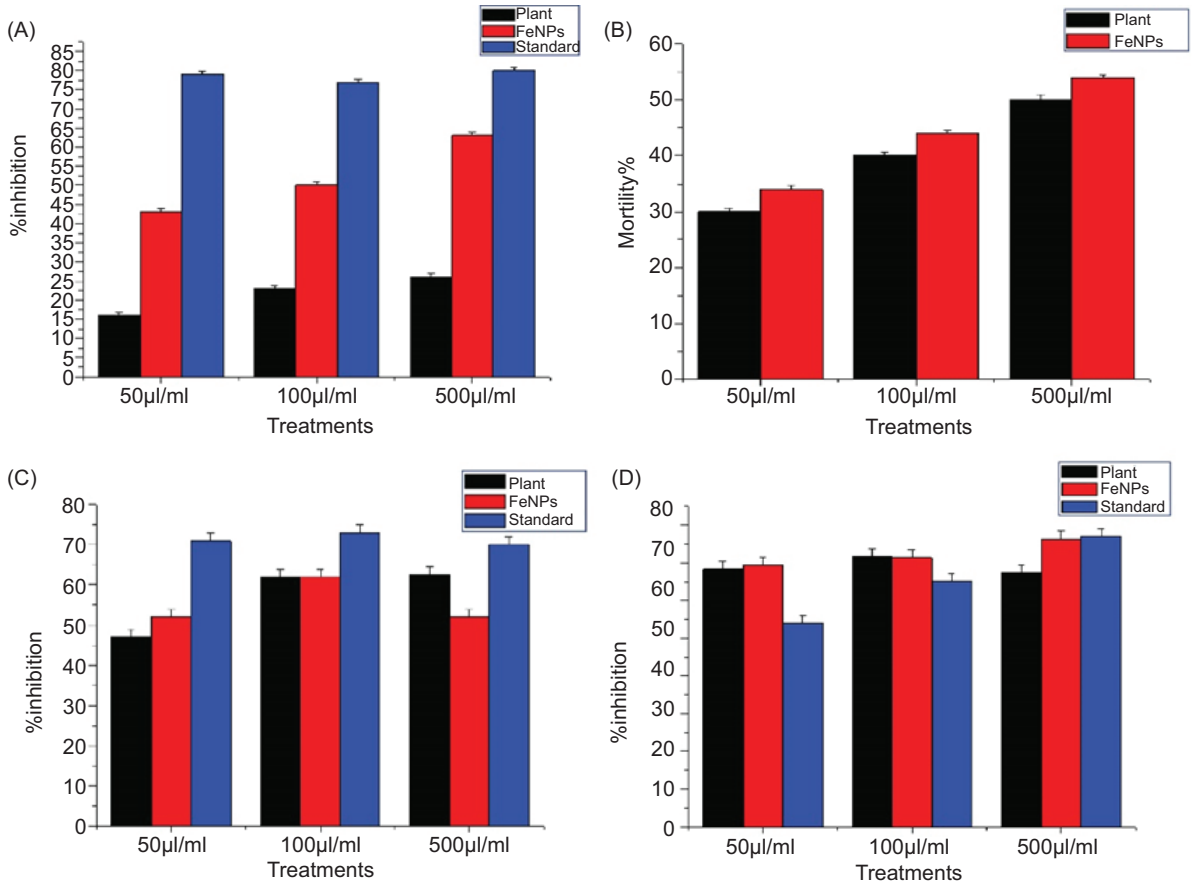

Figure 8. (A) Anti-oxidant graph, (B) Analgesic, (C) Insecticidal, and (D) phytotoxic activity of FeNPs synthesized using *Grewia optiva* extract.

rate was significantly ($p < 0.0001$) observed with FeNPs at 500 µl/mL, resulting in a 69% mortality rate. This was followed by the leaf extract of *Grewia optiva*, which showed a significant ($p < 0.0001$) mortality rate of 60% at 500 µl/mL, and 57% at 100 µl/mL (Figure 8C).

Muthusamy *et al*. (*2023*) demonstrated strong larvicidal efficacy against *Spodoptera litura* and *Helicoverpa armigera* when fenvalerate was combined with iron nanoparticles produced from *Trigonella foenum-graecum*. Positive results were also observed in the antifeedant effect of *T. foenum-graecum* FeNPs. Ahmed *et al*. (*2023*) reported significant mortality in the growth stages of *Musca domestica* larvae, with mortality rates varying according to the concentration of each treatment. The first larval stage exhibited the highest mortality, followed by the second larval stage and the adult stage. Larvae treated with water (0.3%) showed very low mortality. An inverse relationship was observed between the death rate and synthetic iron concentration, suggesting that concentration plays a crucial role in both larvicidal and adult effects.

Phytotoxic activity

To assess the phytotoxic potential of FeNPs and plant extract (*Grewia optiva*), three different concentrations (50 µl/mL, 100 µl/mL, 500 µl/mL) were used in the experiment. The results showed that FeNPs exhibited a high inhibition rate, with significant ($p<0.0001$) inhibition of 63% at 500 µl/mL. The extract (*Grewia optiva*) showed a 30% inhibition rate at 500 µl/mL, followed by 26% at 100 µl/mL, with both results being significantly ($p<0.0001$) different. The standard herbicide, atrazine, showed a 79% inhibition rate at 500 µl/mL (Figure 8D).

Anti-pyretic activity

Albino mice were used in the Brewer's yeast-induced pyrexia method. The animals were administered 20% Brewer's yeast at a dosage of 20 mL per kilogram of their body weight. The mice were then given different dosages of samples (50 µl/mL, 100 µl/mL, and 500 µl/mL) of *Grewia optiva* extract and FeNPs as shown in Table 1. The body temperature of the mice was measured every hour for 4 h using a lubricated rectal thermometer. In the second hour, the body temperature was regulated by administering 500 µl/mL of FeNPs, followed by the extract.

The oral administration of Ephedra-AuNPs at dosages of 8, 16, and 32 g, as well as the oral administration of Ephedra-Gypsum at dosages of 8, 16, and 32 g, was studied by *Chaudhary et al.* (2023). A noticeably lower temperature was observed depending on the dosage given. The antipyretic effect of Ephedra-AuNPs at 32 µg/g/day began within the first hour ($p < 0.01$) and lasted for 8 h ($p < 0.05$).

Conclusion

The green method for synthesizing iron nanoparticles was carried out at room temperature using *Grewia optiva* leaf extract as an effective source for FeNPs production. UV spectrophotometry of FeNPs revealed maximum absorbance in the range of 400 nm to 500 nm, confirming the formation of FeNPs. XRD analysis indicated that the FeNPs had a face-centered cubic (FCC) crystalline structure. FT-IR spectroscopy highlighted the reduction and capping agents (functional groups) involved in the synthesis. SEM imaging showed monodispersed nanoparticles, while TEM analysis confirmed the size of the FeNPs. The antibacterial and antifungal activities of the bio-fabricated FeNPs demonstrated their effective antimicrobial properties. Additionally, the free radical scavenging (antioxidant) potential of the FeNPs showed high antioxidant activity. Furthermore, FeNPs exhibited

Table 1. Anti-pyretic activity of FeNPs synthesized using *Grewia optiva* leaves extract.

Drug	Dose (µl/ mL or mg/ mL)	Temperature(^{0}F) before applying yeast	Temperature noted after applying the samples				
			0 h	1 h	2 h	3 h	4 h
Plant Extract (*Grewia optiva)*	50µl/mL, 100µl/ mL, 500µl/ mL	97	100 99.4 99.8	99 99.2 99.7	100 98.5 99.4	100 99 99	100.5 99.3 99.6
FeNPs	50µl/mL, 100µl/mL, 500µl/mL	97	100 100 99.3	100 92.5 99.2	100.3 98.4 99.4	100.6 98.2 99.2	100.3 98.5 99
Positive control Paracetaol	1 mg/mL	97	100 100 98	100.5 99.5 99	100 99.5 99.2	100 99.5 99	100.5 99.4 99
Negative control (normal saline)	10% v/v	97	101.5	101 5	101 5	101 5	101.5

significant phytotoxic, insecticidal, as well as analgesic and antipyretic properties.

Acknowledgments

The present study was financed by project MECESUP UCT 0804, May 2023.

Data Availability Statement

Original contributions presented in the study are included in the article. Further inquiries can be directed to the corresponding authors.

Author Contributions

K.A., M.S.K., S.A., and M.A.K.: conceived and designed the research. K.A., M.S.K., S.A., and F.B.: performed the experiments. M.B., P.R.D.R-E., M.A.K., S.A., H.B., and C.T.: analyzed and interpreted the data. All authors contributed equally to the preparation, revision, and final approval of the manuscript for submission.

Conflicts of Interest

The authors declare no conflict of interest.

References

Acay, H. (2021). Utilization of Morchella esculenta-mediated green synthesis golden nanoparticles in biomedicine applications. Preparative Biochemistry & Biotechnology, 51(2), 127–136. https://doi.org/10.1080/10826068.2020.1799390

Ahmed, M.S., Begum, H., & Kim, Y.B. (2020). Iron nanoparticles implanted metal-organic-frameworks based Fe–N–C catalysts for high-performance oxygen reduction reaction. Journal of Power Sources, 451, 227733. https://doi.org/10.1016/j.jpowsour.2020.227733

Ahmed, S.H., Hameed, R.S., Yousif, A.M., & Jazar, Z.H. (2023). Studying the antibacterial and insecticidal properties of rosemary extract by iron nanoparticles prepared by using ultrasound. South Asian Research Journal of Applied Medical Sciences, 5(2), 19–25. https://doi.org/10.36346/sarjams.2023.v05i02.001

Akhbari, M., Hajiaghaee, R., Ghafarzadegan, R., Hamedi, S., & Yaghoobi, M. (2019). Process optimisation for green synthesis of zero-valent iron nanoparticles using Mentha piperita. IET Nanobiotechnology, 13(2), 160–169. https://doi.org/10.1049/iet-nbt.2018.5040

ALISHA, AS., & Thangapandiyan, S. (2019). Comparative bioassay of silver nanoparticles and malathion on infestation of red flour beetle, Tribolium castaneum. The Journal of Basic and Applied Zoology, 80, 1–10. https://doi.org/10.1186/s41936-019-0124-0

Asad, K., Shams, S., Ibáñez-Arancibia, E., De los Ríos-Escalante, P.R., Badshah, F., Ahmad, F., Khan, M.S., & Khan, A. (2024). Anti-inflammatory, antipyretic, and analgesic potential of chitin and chitosan derived from cockroaches (*Periplaneta americana*) and termites. Journal of Functional Biomaterials, 15, 80. https://doi.org/10.3390/jfb15030080

Asad, S., Anwar, N., Shah, M., Anwar, Z., Arif, M., Rauf, M., Ali, K., Shah, M., Murad, W., Albadrani, G.M., & Altyar, A.E. (2022). Biological synthesis of silver nanoparticles by Amaryllis vittata (L.) Herit: from antimicrobial to biomedical applications. Materials, 15(16), 5478. https://doi.org/10.3390/ma15165478

Bhuiyan, M.S.H., Miah, M.Y., Paul, S.C., Aka, T.D., Saha, O., Rahaman, M.M., Sharif, M.J.I., Habiba, O., & Ashaduzzaman, M. (2020). Green synthesis of iron oxide nanoparticle using Carica papaya leaf extract: application for photocatalytic degradation of remazol yellow RR dye and antibacterial activity. Heliyon, 6(8), https://doi.org/10.1016/j.heliyon.2020.e04603

Buarki, F., AbuHassan, H., Al Hannan, F., & Henari, F.Z. (2022). Green synthesis of iron oxide nanoparticles using Hibiscus rosa sinensis flowers and their antibacterial activity. Journal of Nanotechnology, 2022(1), 5474645. https://doi.org/10.1155/2022/5474645

Chaudhary, P., Sharma, R., Rawat, S., & Janmeda, P. (2023). Antipyretic medicinal plants, phytocompounds, and green nanoparticles: an updated review. Current Pharmaceutical Biotechnology, 24(1), 23–49. https://doi.org/10.2174/1389201023666220330005020

Chopra, H., Bibi, S., Mishra, A.K., Tirth, V., Yerramsetty, S.V., Murali, S.V., Ahmad, S.U., Mohanta, Y.K., Attia, M.S., Algahtani, A., & Islam, F. (2022). Nanomaterials: a promising therapeutic approach for cardiovascular diseases. Journal of Nanomaterials, 2022(1), 4155729. https://doi.org/10.1155/2022/4155729

Dash, A., Ahmed, M.T., & Selvaraj, R. (2019). Mesoporous magnetite nanoparticles synthesis using the Peltophorum pterocarpum pod extract, their antibacterial efficacy against pathogens and ability to remove a pollutant dye. Journal of Molecular Structure, 1178, 268–273. https://doi.org/10.1016/j.molstruc.2018.10.042

Dastagir, G. & Hussain, F. (2013). Phytotoxic and insecticidal activity of plants of family Zygophyllaceae and Euphorbiaceae. Sarhad Journal of Agriculture, 29(1), 83–91. https://doi.org/10.5897/jmpr12.539

Demirezen, D.A., Yıldız, Y.Ş., & Yılmaz, D.D. (2019). Amoxicillin degradation using green synthesized iron oxide nanoparticles: Kinetics and mechanism analysis. Environmental Nanotechnology, Monitoring & Management, 11, 100219. https://doi.org/10.1016/j.enmm.2019.100219

Ebrahiminezhad, A., Zare-Hoseinabadi, A., Berenjian, A., & Ghasemi, Y. (2017). Green synthesis and characterization of zero-valent iron nanoparticles using stinging nettle (*Urtica dioica*) leaf extract. Green Processing and Synthesis, 6(5), 469–475. https://doi.org/10.1515/gps-2016–0133

Hammad, E.N., Salem, S.S., Mohamed, A.A., & El-Dougdoug, W. (2022). Environmental impacts of ecofriendly iron oxide nanoparticles on dyes removal and antibacterial activity. Applied Biochemistry and Biotechnology, 194(12), 6053–6067. https://doi.org/10.1007/s12010-022-04105-1

Hooda, R. & Sharma, M. (2020). Green synthesis, characterization and antibacterial activity of iron oxide nanoparticles. Plant Archives, https://doi.org/10.21203/rs.3.rs-3808096/v1

Iftikhar, M., Zahoor, M., Naz, S., Nazir, N., Batiha, G.E.S., Ullah, R., Bari, A., Hanif, M. & Mahmood, H.M. (2020). Green synthesis of silver nanoparticles using *Grewia optiva* leaf aqueous extract and isolated compounds as reducing agent and their biological activities. Journal of Nanomaterials, 2020(1), 8949674. https://doi.org/10.1155/2020/8949674

Jagaran, K. & Singh, M., 2020. Nanomedicine for COVID-19: potential of copper nanoparticles. Biointerface Research in Applied Chemistry, 11(3), 10716–10728. https://doi.org/10.33263/briac113.1071610728

Kalashgarani, M.Y. & Babapoor, A. (2022). Application of nano-antibiotics in the diagnosis and treatment of infectious diseases. Advances in Applied NanoBio-Technologies, 3(1), 22–35. https://doi.org/10.1016/b978-0-323-91201-3.00008-6

Karpagavinayagam, P. & Vedhi, C. (2019). Green synthesis of iron oxide nanoparticles using Avicennia marina flower extract. Vacuum, 160, 286–292. https://doi.org/10.1016/j.vacuum.2018.11.043

Keshari, A.K., Srivastava, R., Singh, P., Yadav, V.B. & Nath, G. (2020). Antioxidant and antibacterial activity of silver nanoparticles synthesized by Cestrum nocturnum. Journal of Ayurveda and Integrative Medicine, 11(1), 37–44. https://doi.org/10.1016/j.jaim.2017.11.003

Keshari, A.K., Srivastava, R., Singh, P., Yadav, V.B., & Nath, G. (2020). Antioxidant and antibacterial activity of silver nanoparticles synthesized by Cestrum nocturnum. Journal of Ayurvedic Herbal and Integrative Medicine, 11(1), 37–44. https://doi.org/10.1016/j.jaim.2017.11.003 PMid:30120058.

Khan, D.A., Ali, Z., Iftikhar, S., Amraiz, D., Zaidi, N.U.S.S., Gul, A., & Babar, M.M. (2018). Role of phytohormones in enhancing antioxidant defense in plants exposed to metal/metalloid toxicity. Plants Under Metal and Metalloid Stress: Responses, Tolerance and Remediation, 367–400.

Liu, A., Liu, J., Pan, B., & Zhang, W.X. (2014). Formation of lepidocrocite (γ-FeOOH) from oxidation of nanoscale zero-valent iron (nZVI) in oxygenated water. RSC Advances, 4(101), 57377–57382. https://doi.org/10.1039/c4ra08988j

Mirza, A.U., Kareem, A., Nami, S.A., Khan, M.S., Rehman, S., Bhat, S.A., Mohammad, A., & Nishat, N. (2018). Biogenic synthesis of iron oxide nanoparticles using Agrewia optiva and Prunus persica phyto species: Characterization, antibacterial and antioxidant activity. Journal of Photochemistry and Photobiology B: Biology, 185, 262–274. https://doi.org/10.1016/j.jphotobiol.2018.06.009

Mofolo, M.J., Kadhila, P., Chinsembu, K.C., Mashele, S., & Sekhoacha, M. (2020). Green synthesis of silver nanoparticles from extracts of Pechuel-loeschea leubnitziae: their anti-proliferative activity against the U87 cell line. Inorganic Nano-Metal Chemistry, 50(10), 949–955. https://doi.org/10.1080/24701556.2020.1729191

Muthusamy, R., Ramkumar, G., Kumarasamy, S., Chi, N.T.L., Al Obaid, S., Alfarraj, S. & Karuppusamy, I. (2023). Synergism and toxicity of iron nanoparticles derived from Trigonella foenum-graecum against pyrethriod treatment in S. litura and H. armigera (Lepidoptera: Noctuidae). Environmental Research, 231, 116079. https://doi.org/10.1016/j.envres.2023.116079

Nahari, M.H., Al Ali, A., Asiri, A., Mahnashi, M.H., Shaikh, I.A., Shettar, A.K. & Hoskeri, J. (2022). Green synthesis and characterization of iron nanoparticles synthesized from aqueous leaf extract of vitex leucoxylon and its biomedical applications. Nanomaterials, 12(14), 2404. https://doi.org/10.3390/nano12142404

Naseem, T. & Farrukh, M.A. (2015).Antibacterial activity of green synthesis of iron nanoparticles using Lawsonia inermis and Gardenia jasminoides leaves extract. Journal of Chemistry, 2015(1), 912342. https://doi.org/10.1155/2015/912342

Omidian, H., Babanejad, N., & Cubeddu, L.X. (2023). Nanosystems in cardiovascular medicine: advancements, applications, and future perspectives. Pharmaceutics, 15(7), 1935. https://doi.org/10.3390/pharmaceutics15071935

Păduraru, D.N., Ion, D., Niculescu, A.G., Mușat, F., Andronic, O., Grumezescu, A.M. & Bolocan, A. (2022). Recent developments in metallic nanomaterials for cancer therapy, diagnosing and imaging applications. Pharmaceutics, 14(2), 435. https://doi.org/10.3390/pharmaceutics14020435

Prakash, M., Chandraprabha, M.N., Krishna, R.H., Satish, H., & Kumar, S.G. (2024). Iron oxide nanoparticles for inflammatory bowel disease: Recent advances in diagnosis and targeted drug therapy. Applied Surface Science, 19, 100540. https://doi.org/10.1016/j.apsadv.2023.100540

Priya, Naveen, Kaur, K., & Sidhu, A.K. (2021). Green synthesis: An eco-friendly route for the synthesis of iron oxide nanoparticles. Frontiers in Nanotechnology, 3, 655062. https://doi.org/10.3389/fnano.2021.655062

Qamar, M., Akhtar, S., Ismail, T., Wahid, M., Barnard, R.T., Esatbeyoglu, T., & Ziora, Z.M. (2021). The chemical composition and health-promoting effects of the Grewia species—A systematic review and meta-analysis. Nutrients, 13(12), 4565. https://doi.org/10.3390/nu13124565

Roy, A., Singh, V., Sharma, S., Ali, D., Azad, A.K., Kumar, G., & Emran, T.B. (2022). Antibacterial and dye degradation activity of green synthesized iron nanoparticles. Journal of Nanomaterials., 2022(1), 3636481. https://doi.org/10.1155/2022/3636481

Sajid, M. & Płotka-Wasylka, J. (2020). Nanoparticles: Synthesis, characteristics, and applications in analytical and other sciences. Microchemical Journal, 154, 104623. https://doi.org/10.1016/j.microc.2020.104623

Sandhya, J., Veeralakshmi, S., & Kalaiselvam, S. (2021). Tripolyphosphate crosslinked Triticum aestivum (wheatgrass) functionalized antimicrobial chitosan: Ameliorating effect on physicochemical, mechanical, invitro cytocompatibility and cell migration properties. Journal of Biomolecular Structure and Dynamics, 39(5), 1635–1644. https://doi.org/10.1080/07391102.2020.1736160

Shah, M., Murad, W., Ur Rehman, N., Halim, S.A., Ahmed, M., Rehman, H., Zahoor, M., Mubin, S., Khan, A., Nassan, M.A., & Batiha, G.E.S. (2021). Biomedical applications of Scutellaria edelbergii Rech. f.: in vitro and in vivo approach. Molecules, 26(12), 3740. https://doi.org/10.3390/molecules26123740

Sulaiman, S., Ahmad, S., Naz, S.S., Qaisar, S., Muhammad, S., Alotaibi, A., & Ullah, R. (2022). Synthesis of copper oxide-based nanoformulations of etoricoxib and montelukast and their evaluation through analgesic, anti-inflammatory, anti-pyretic, and acute toxicity activities. Molecules, 27(4), 1433. https://doi.org/10.3390/molecules27041433

Sultana, T., Malik, K., Raja, N.I., Sohail, Hameed, A., Ali, A., Mashwani, Z.U.R., Baloch, M.Y.J. & Alrefaei, A.F. (2023). Phytofabrication, characterization, and evaluation of novel bio-inspired selenium–iron (Se–Fe) nanocomposites using Allium sativum extract for bio-potential applications. Green Processing and Synthesis, 12(1), 20230049. https://doi.org/10.1515/gps-2023-0049

Tan, B., Chen, J. & Wang, W. (2023). Evaluation of the analgesic and anesthetic properties of silver nanoparticles supported over biodegradable acacia gum-modified magnetic nanoparticles. Open Chemistry, 21(1), 20230180. https://doi.org/10.1515/chem-2023-0180

Üstün, E., Önbaş, S.C., Çelik, S.K., Ayvaz, M.Ç. & Şahin, N. (2022). Green synthesis of iron oxide nanoparticles by using Ficus carica leaf extract and its antioxidant activity. Biointerface Research in Applied Chemistry, 12(2), 2108–2116. https://doi.org/10.33263/briac122.21082116

Wei, Y., Fang, Z., Zheng, L., Tan, L., & Tsang, E.P. (2016). Green synthesis of Fe nanoparticles using Citrus maxima peels aqueous extracts. Materials Letters, 185, 384–386. https://doi.org/10.1016/j.matlet.2016.09.029

Xu, W., Yang, T., Liu, S., Du, L., Chen, Q., Li, X., Dong, J., Zhang, Z., Lu, S., Gong, Y., & Zhou, L. (2022). Insights into the Synthesis, types and application of iron Nanoparticles: The overlooked significance of environmental effects. Environmental International, 158, 106980. https://doi.org/10.1016/j.envint.2021.106980

Younis, N.K., Ghoubaira, J.A., Bassil, E.P., Tantawi, H.N., & Eid, A.H. (2021). Metal-based nanoparticles: Promising tools for the management of cardiovascular diseases. Nanomedicine (N. Y., NY, U. S.), 36, 102433. https://doi.org/10.1016/j.nano.2021.102433